ORIGINAL PAPER

Physical and Mechanical Properties of Granite After High-Temperature Treatment

Yan Qin[1] · Hong Tian[2] · Neng-Xiong Xu[1] · Yu Chen[1]

Abstract

As granite is one of the most widely encountered lithologies in studies of high-temperature rock mechanics, the effects of high temperatures on the physical and mechanical properties of granite have attracted considerable attention. In this study, to identify the physical and mechanical properties of granite observed before and after high-temperature treatment from room temperature to 1000 °C and to determine the influence of high temperatures on granite and on its intrinsic connections, appearance, and mineral morphology, longitudinal wave testing and uniaxial and triaxial tests were performed. Our primary conclusions are as follows: (1) effects of high temperatures on microscopic minerals of granite primarily include the oxidation of dark minerals, the recrystallization of feldspar minerals, and the generation and extension of mineral cracks. (2) High temperatures decrease the speed of longitudinal waves in granite and cause longitudinal wave energy to be absorbed. Cracks created by high temperatures cause longitudinal waves to not be detected. (3) Relationships between stress and strain processes at 400 °C in granite first soften and subsequently harden, and mechanical properties change only slightly overall. After a temperature of 400 °C is reached, with increasing temperatures, softening characteristics emerge. At 800 °C, plastic deformation occurs. At 1000 °C, the strength and deformability of rock specimens are largely diminished. We found 600 °C to be the threshold of mechanical properties and the transition temperature of the failure mode. (4) Finally, 400 °C, 600 °C, and 800 °C were found to be characteristic temperatures of three different stages of physical and mechanical properties for granite.

Keywords High temperature · Granite · Physical properties · Mechanical properties

List of Symbols

T	Temperature
η_m	Mass loss rate
η_V	Volume growth rate
η_ρ	Density reduction rate
m_1	The mass of the original rock specimen
V_1	The volume of the original rock specimen
ρ_1	The density of the original rock specimen
m_2	The mass of the rock specimen after high-temperature treatment
V_2	The volume of the rock specimen after high-temperature treatment
ρ_2	The density of the rock specimen after high-temperature treatment
σ_1	Axial stress
σ_3	Confining pressure
E	Elastic modulus
ε	Axial strain
UCS	Uniaxial compressive strength
c	Cohesion
φ	Friction angle
v_{p0}	Longitudinal wave velocity of the original rock specimen
v_{pT}	Longitudinal wave velocity of the rock specimen treated at each temperature
σ_0	Axial stress of the original rock specimen
σ_T	Axial stress of the rock specimen treated at each temperature
E_0	Elastic modulus of the original rock specimen
E_T	Elastic modulus of the rock specimen treated at each temperature
ε_0	Axial strain of the original rock specimen

✉ Neng-Xiong Xu
  xunengxiong@cugb.edu.cn

1   School of Engineering and Technology, China University of Geosciences (Beijing), Xueyuan Road 29, Beijing 100083, People's Republic of China

2   Faculty of Engineering, China University of Geosciences (Wuhan), Lumo Road 388, Wuhan 430074, People's Republic of China

ε_T	Axial strain of the rock specimen treated at each temperature
φ_0	Friction angle of the original rock specimen
φ_T	Friction angle of the rock specimen treated at each temperature
c_0	Cohesion of the original rock specimen
c_T	Cohesion of the rock specimen treated at each temperature
$D(v_p)$	Damage factors in terms of longitudinal wave velocity
$D(\text{UCS})$	Damage factors in terms of uniaxial compressive strength
$D(E)$	Damage factors in terms of the elastic modulus
$D(\varepsilon)$	Damage factors in terms of peak strain
$D(\varphi)$	Damage factors in terms of friction angle
$D(c)$	Damage factors in terms of cohesion

1 Introduction

High-temperature rock mechanics have received increasing attention in recent years, especially with respect to projects related to coal mining, oil and gas storage, geothermal development, and nuclear waste disposal. The change rules and mechanisms of the physical and mechanical properties of rocks subjected to high temperatures have become a focus of research in rock mechanics (Basu et al. 2013; Chmel 2013; Costamagna et al. 2007; Dwivedi et al. 2008; Goodman 1989; Hardy 1972; Hawkes and Mellor 1970; Kawakata et al. 1999; Mitchell et al. 2016; Rudajev et al. 2000; Shao et al. 2014; Vázquez et al. 2015; Xu et al. 2014; Zhao et al. 2012, 2013).

At present, many research discoveries regarding the effects of high temperatures on the physical and mechanical properties of rocks have already been made. The rocks examined in previous studies include calcareous limestone (Brotons et al. 2013), mudstone (Mao et al. 2015), claystone (Tian et al. 2014), marble (Liu and Xu 2013), sandstone (Liu and Xu 2015; Liu et al. 2016; Tian et al. 2012, 2016; Yang et al. 2017a, b; Sirdesai et al. 2018), diorite (Tian et al. 2017), tephrite (Ersoy et al. 2017), and granite. Because granite is one of the most common rocks in high-temperature rock mechanics projects, the study results on granite are also extensive.

Because the complexities of granite's mineral composition and the thermal expansion coefficients of different minerals vary, mineral expansion occurring at high temperatures applies significant levels of thermal stress between minerals, resulting in crack formation within rock and seriously affecting rock mechanical properties (Takarli et al. 2008). Physical and chemical changes occurring in different minerals under the effects of high temperatures also vary, and the original structures of the minerals are damaged by those irreversible changes. Therefore, how the mechanical properties of

granite develop after high temperatures and how the stability of rock engineering can, in turn, be evaluated are critical concerns for engineers working in this field.

Several experimental studies on granites subjected to high temperatures have revealed changes in physical and mechanical properties relative to those of undisturbed granite:

1. Regarding microscopic research on the minerals, the main approach applied involves observing the development of microscopic cracks in granite after applying high temperatures using light microscopy and scanning electron microscopy (SEM). Homand-Etienne and Houpert (1989) found that as temperatures increase, the lengths of cracks remain nearly unchanged, while crack widths increase. Chen et al. (2017) found that under high-temperature catalysis, mica is oxidized, and its mineral morphology changes from unstable 3T or 1M to stable 2M1. Using light microscopy, Yang et al. (2017a, b) found that at 400 °C, intercrystalline cracks form at the boundaries between quartz and feldspar; that at 600 °C, transgranular cracks appear on quartz and feldspar minerals; and that at 700 °C, visible cracks appear on the surfaces of rock specimens. Using SEM, Huang et al. (2017) observed that primary cracks in granite close at 150 °C, strengthening the granite structure; that crystal boundary cracks form at 300 °C; that transgranular cracks form at 600 °C; and that cracks form on rock surfaces at 900 °C.

2. Many studies have examined physical properties with respect to changes in mass, volume, density, elastic wave velocity, porosity, and permeability. Huang et al. (2017) showed that as temperatures increase, mass loss, volume growth, and density reduction rates gradually increase. At 900 °C, the mass loss rate was measured to be approximately 0.35%, the volume growth rate was measured to be approximately 3.8%, and the density reduction rate was measured to be approximately 3.9%. Zhang et al. (2016) concluded that the decrease in mass observed was mainly caused by a loss of interlayer (105 °C), zeolite (200–300 °C), crystalline (400 °C), and structural water (above 600 °C). Liu and Xu (2015) found that the longitudinal wave velocity of granite decreases linearly with an increase in temperature to 1000 °C and that changes in granite density to 800 °C are not significant but decrease significantly at 1000 °C. Yang et al. (2017a, b) found that porosity increases by approximately 3.46% at 800 °C and that permeability also increases significantly.

3. In terms of mechanical properties, Liu and Xu (2015) found that compressive strength and elastic modulus values gradually decrease with increasing temperatures. Chen et al. (2017) found that compressive strength levels increase at 200 °C and decline with increasing temperature beyond 200 °C. Chen et al. (2017) also found

that Young's modulus decreases linearly with temperature below 600 °C and remains unchanged above 600 °C, and fracture toughness gradually decreases with increasing temperature. Hu et al. (2018) divided the temperature range between room temperature and 1000 °C into four stages (20–200 °C, 200–400 °C, 400–600 °C, and 600–1000 °C), and found that tensile strength and fracture toughness increase as temperatures rise below 200 °C and decrease rapidly above 200 °C, that compressive strength and elastic modulus values decline above 400 °C and that the rock damage rate increases rapidly above 400 °C. Yang et al. (2017a, b) showed that as temperatures increase, the uniaxial compressive strength, crack threshold strength, and static modulus of elasticity increase first and later decrease, while the dynamic elastic modulus gradually decreases. The dynamic Poisson ratio remains unchanged, while the static Poisson's ratio gradually decreases below 640 °C and later increase rapidly. Scherbakov and Chmel (2014) and Xu and Zhang (2018) used acoustic emission (AE) technologies to find that under loading conditions, AE energy levels increase with increasing temperatures. Kumari et al. (2017) found that at temperatures below 300 °C, as temperatures increase, the elastic modulus, peak deviation stress, and internal friction angle values increase with increasing temperatures and cohesion levels first increase and then decrease. However, cohesion values observed at 300 °C were still found to be greater than those of undisturbed granite.

4. In other areas, Yin et al. (2016) found that compared to granite observed after high-temperature treatment, the brittle-to-critical transition temperature of granite under high temperature was lower and presented a lower peak stress value, while the peak strain value was found to be larger. Su et al. (2017) studied rock burst characteristics of granite after high-temperature treatment from an energy perspective, and found that at 300 °C, mechanical properties change, while rock burst energy levels are the highest. At temperatures below 500 °C, granite exhibits considerable rock burst energy levels, but these levels decrease above 600 °C. In addition, several publications have focused on the numerical simulation of high-temperature granite engineering and have offered valuable conclusions (Kumari et al. 2017; Shao et al. 2015; Hoxha and Homand 2000).

Most of the studies described above have focused on microscopic damage or macromechanical properties of high-temperature granite. Research on the physical and mechanical properties of rocks subjected to high temperatures via both basic physical property measurements and mineral variation on a microscale (under a light microscope) is currently limited. In addition, most studies have used temperature intervals of 200 °C, which are notably large. Therefore, the definition of the physical and mechanical property threshold

of granite must be further verified. This study further refined the temperature intervals to 20 °C, 100 °C, 200 °C, 300 °C, 400 °C, 500 °C, 600 °C, 800 °C, and 1000 °C; experimentally examined granite physical and mechanical properties, including mass, volume, density, the appearance of cracks, mineral structure, longitudinal wave velocity and amplitude, compressive strength, modulus of elasticity, peak strain, cohesion, friction angle, and failure mode; and revealed the influence of high temperatures on the physical and mechanical properties of granite and on its intrinsic connections.

2 Rock Specimens and Experiments

2.1 Specimen Characterization

The granite specimens used in this experimental study were collected from Fangshan District in Beijing, China. The granite specimens were gray, with an average density of 2.72 g/cm^3 and an average longitudinal wave velocity of approximately 4800 m/s. The mineral composition of the specimens was 38% quartz, 47% plagioclase, 11% microcline, and 4% mica by XRD. To avoid the influence of heterogeneity, all granite specimens were drilled in the same direction from a block of the granite mass as the International Society for Rock Mechanics and Rock Engineering (ISRM 2007) suggested. After cutting, 108 cylindrical specimens (φ 25 mm × 50 mm) were obtained, and the rock specimens were found to adhere to the specifications of ISRM (ISRM 2007).

Given that during the deep underground disposal of nuclear waste granite, temperatures do not generally exceed 500 °C, we examined changes in the physical and mechanical properties of granite to 500 °C in detail. Temperatures of up to 500 °C were examined at 100 °C intervals, and an interval of 200 °C was used above 600 °C. Thus, we studied processes observed at temperatures of 20 °C, 100 °C, 200 °C, 300 °C, 400 °C, 500 °C, 600 °C, 800 °C, and 1000 °C. In addition, based on an estimation of the depth of buried nuclear waste and of rock density values, 15 MPa was set as the upper confining pressure limit, and 5 MPa was set as the confining pressure interval.

2.2 Test Procedures

We used an electronic balance (accuracy level of 0.001 g), a Vernier caliper (50°), a longitudinal wave tester (DSG-1, 50 kHz), a high-temperature furnace (SG-XL1200, maximum heating temperature of 1200 °C and temperature control accuracy of ± 3 °C), an optical microscope (2084BS53, 20×), and a mechanical tester (TAW-2000) in this study. To ensure the reliability of the experimental results, the number of experimental rock specimens examined under the same experimental conditions was set to 3. Test procedures applied to each rock specimen were as follows:

1. Specimens were placed in a ventilated area at room temperature for 2 weeks to eliminate the effects of natural moisture content.
2. The initial physical properties of the rock specimens were measured prior to heating (i.e., measurement mass, size, and longitudinal wave).
3. Each rock specimen was placed in a high-temperature furnace in accordance with the temperature group for heat treatment, and the heating rate was set to 3 °C/min. After heating to the target temperature, the furnace was programmed to maintain a constant temperature for 2 h. Then, the power was turned off, and the rock specimens were naturally cooled to room temperature in the furnace.
4. The rock specimens were removed after high-temperature treatment, and the quality, size, and longitudinal wave of each rock specimen were measured.
5. One piece of spare rock in each temperature group was taken as a probe to observe mineral morphologies under a light microscope.
6. Uniaxial and triaxial compression tests of the rock specimens were performed using a mechanical tester in accordance with ISRM specifications.

3 Results and Discussion

The experimental results mainly cover the following: (1) the appearance of changes in the rock specimens; (2) changes in microscopic minerals; (3) changes in quality, volume, and density values; (4) changes in longitudinal wave velocity and waveform; (5) stress–strain relations; (6) changes in compressive strength, elastic modulus, and peak strain values; (7) changes in cohesion and friction angles; (8) damage parameters; and (9) failure patterns (Table 1).

3.1 Cracks on the Rock Specimens

Due to the different thermal expansion coefficients of minerals in granite, uneven expansion occurred under high temperatures; thus, cracks appeared on the surface of the granite at 800 °C and 1000 °C (Fig. 1), and cracks formed in the granite at 1000 °C were clearly more abundant and larger than those observed at 800 °C. Huang et al. (2017) found no cracks on the surfaces of rock specimens treated at 800 °C with the naked eye, while obvious cracks formed at 900 °C. Yang et al. (2017a, b) used CT to find that granite forms cracks no larger than 30 μm at 600 °C, that the surfaces of rock specimens crack at 700 °C, and that surface cracks expand at 800 °C. Therefore, granite first forms surface cracks at a temperature of approximately 800 °C.

In addition, when the same group of rock specimens were hit against one another, the 20–500 °C rock specimens

emitted crisp sounds. However, rock specimens treated at 600 °C emitted a softer sound when hit against one another. The softer sounds recorded became more pronounced at 800 °C and very clear at 1000 °C. These results show that a decrease in the density of the rock specimens and an increase in the number of pores were the main factors causing the timbre of the rock specimens to change.

3.2 Changes in Microscopic Minerals

Under a light microscope at 20× magnification, the structures of the specimens and minerals observed after high-temperature treatment at 300 °C (Fig. 2a–d) did not change. At 400 °C and 500 °C (Fig. 2e, f), boundary cracks (marked as 'bc' in the figures) formed at the boundaries between quartz and feldspar, but no transgranular cracks were observed on any mineral. Yang et al. (2017a, b) also observed mineral boundary cracks at 400 °C through an optical microscope, whereas Huang et al. (2017) used CT to find boundary cracks on mineral edges at 300 °C. The fact that we did not observe boundary cracks at 300 °C may be attributed to the effects of our observation scale or to our use of rock specimens of different sources.

At 600 °C (Fig. 2g, h), transgranular cracks (marked as 'tc' in the figures) began to appear on the surfaces of the feldspar, but the cracks were thin, short in length, and less plentiful. The quartz boundary was blurred, and white spots formed on the surface of the feldspar, indicating that recrystallization had occurred. The biotite turned brown, as biotite is a dark-colored mineral consisting of Fe^{2+} and other elements. Fe^{2+} was oxidized by oxygen to Fe^{3+} under high-temperature catalytic action. The color of biotite changed, indicating that oxidation had occurred.

At 800 °C (Fig. 2i, j), the number of cracks on the feldspar increased significantly, and the crack widths and lengths increased. Virtually all of the cracks were connected and meshed. Several cracks formed on the quartz and biotite surfaces, and the biotite specimens turned red, denoting a higher degree of oxidation.

At 1000 °C (Fig. 2k, l), the surfaces of the feldspar and quartz were blurred, indicating that strong processes of alteration had taken place. The biotite specimens became redder than they were at 800 °C, and more fractures were observed. After a temperature of 800 °C was reached, fewer cracks were observed on the feldspar surface, and their widths had narrowed. As the melting point of feldspar is approximately 1100 °C, we assumed that the feldspar contained other minerals, decreasing its melting point and causing it to melt and undergo recrystallization, filling the fractures.

In addition, due to the different thermal expansion coefficients of quartz and feldspar, the destruction of the two minerals involved different patterns. The main minerals shown in Fig. 2g, i, k are quartz and biotite. After treatment at temperatures above 600 °C, transgranular cracks

Table 1 Original data table of physical and mechanical properties

Temperature, °C	σ_3, MPa	η_m, %	η_V, %	η_ρ, %	V_P, m/s	E, GPa	$\sigma_1 - \sigma_3$, MPa	ε, %
20	0	0	0	0	4799	14.00	84.80	0.98
	5					13.41	145.23	1.49
	10					18.17	209.68	1.88
	15					19.30	223.78	2.54
100	0	0.011	0.53	5.63	4476	13.26	71.24	1.05
	5					11.39	142.20	1.63
	10					17.28	165.62	1.88
	15					18.52	216.30	1.95
200	0	0.034	1.05	1.02	3883	17.22	80.70	0.91
	5					14.45	138.80	1.45
	10					17.71	168.70	1.64
	15					18.35	204.95	2.10
300	0	0.039	1.09	1.12	3526	13.92	81.27	1.05
	5					16.11	151.98	1.51
	10					16.54	169.29	1.86
	15					18.90	227.30	2.23
400	0	0.064	1.08	1.14	2981	11.43	69.59	0.92
	5					14.59	130.75	1.69
	10					17.74	193.46	1.93
	15					18.66	217.50	2.04
500	0	0.063	1.23	1.36	2587	9.98	67.73	1.18
	5					15.48	151.27	1.62
	10					14.68	174.58	1.98
	15					14.13	192.92	3.70
600	0	0.102	1.46	1.38	1108	8.57	71.65	1.65
	5					16.65	188.37	2.34
	10					13.87	186.76	3.84
	15					15.19	262.54	4.49
800	0	0.256	3.61	3.58	–	5.59	50.09	2.11
	5					10.13	144.87	4.04
	10					10.94	198.47	4.20
	15					11.66	219.26	5.10
1000	0	0.302	5.63	5.56	–	2.39	26.43	2.20
	5					7.32	123.23	4.76
	10					10.31	192.46	5.31
	15					11.50	233.88	5.57

The values of mass, volume, density, and longitudinal wave velocity are the average values of the test performed at atmospheric pressure, and longitudinal waves were not detected at 800 °C and 1000 °C

appeared on quartz surfaces. A large number of smaller cracks were observed. The main mineral shown in Fig. 2h, j, l is feldspar, and cracks observed were wider than those observed on the quartz after treatment at 600 °C.

3.3 Changes in Quality, Volume, and Density

We defined the mass loss rate η_m, volume growth rate η_V, and density reduction rate η_ρ as follows:

$$\eta_m = {(m_1 - m_2)}/{m_1} \times 100\%, \quad \eta_V = {(V_2 - V_1)}/{V_1} \times 100\%,$$
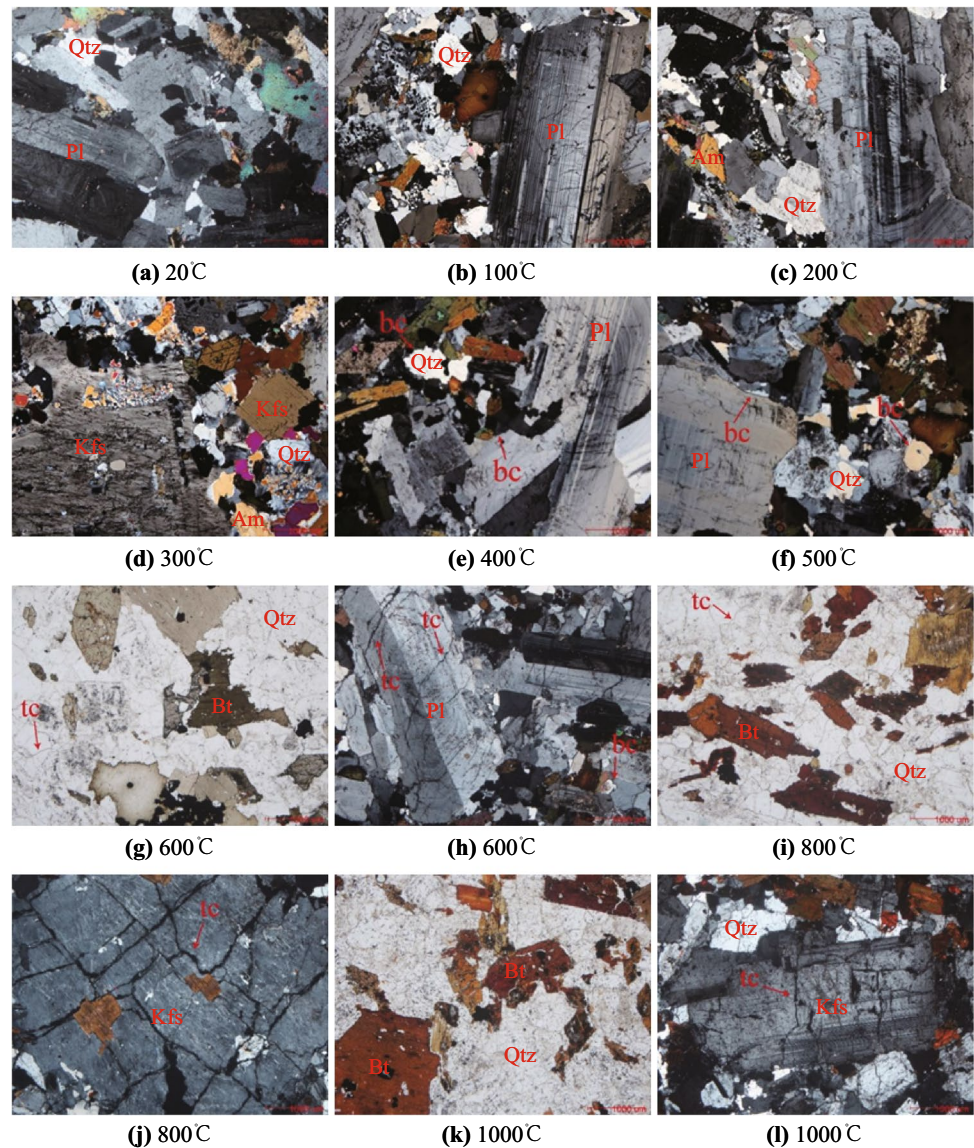$$\eta_\rho = {(\rho_1 - \rho_2)}/{\rho_1} \times 100\%.$$

In these formulas, m_1, V_1, and ρ_1 are the mass, volume, and density of the original rock specimen, respectively, and m_2, V_2, and ρ_2 are the mass, volume, and density of the rock specimen after high-temperature treatment, respectively.

Fig. 1 Cracks formed on the rock specimens after high-temperature treatment at 800 °C and 1000 °C
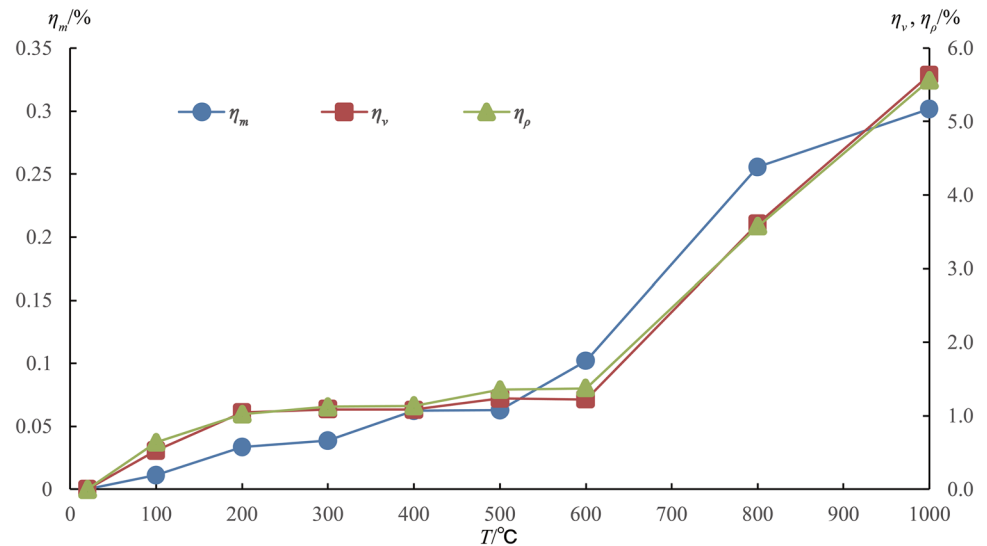
With increasing temperatures, the mass loss, volume growth, and density reduction rates of the granite gradually increased (Fig. 3). Changes observed below 200 °C were obvious, and the mass loss rate continued to increase from 200 to 600 °C, while the volume growth rate and density reduction rate changed little. When temperatures exceeded 600 °C, the mass loss rate, volume growth rate, and density reduction rate increased dramatically.

The mass loss rate observed at 200 °C was 0.034%, while at 200–300 °C, the rate remained virtually unchanged. Interlayer water generally evaporated at approximately 100 °C; thus, interlayer water was completely absent at 200 °C, and losses of zeolite water were not significant at 200–300 °C. At 400 °C, the mass loss rate further increased to 0.064%. At 500 °C, the loss rate stabilized. We thus assume that zeolite water was completely absent at 400 °C, while there was almost no loss of bound water from 400 to 500 °C. The

Fig. 2 Illustration of minerals in the rock specimens observed after treatment at different temperatures under a light microscope

(a) 20℃ (b) 100℃ (c) 200℃
(d) 300℃ (e) 400℃ (f) 500℃
(g) 600℃ (h) 600℃ (i) 800℃
(j) 800℃ (k) 1000℃ (l) 1000℃

Fig. 3 Relationships between η_m, η_V, and η_ρ and temperature

mass loss rate increased significantly above 500 °C, indicating that internal minerals of the rock specimens underwent significant physical and chemical changes, while crystalline water volumes declined through mineral dehydration, and structural water volumes declined as a result of dehydroxylation (Zhang et al. 2016). Mass loss rates were measured to be 0.102% at 600 °C and 0.256% at 800 °C, and were highest at 600–800 °C, indicating that chemical changes were most dramatic within this range of temperatures. From 800 to 1000 °C, the mass loss rate slightly stabilized, indicating that chemical changes were still occurring, and the mass loss rate reached 0.302% at 1000 °C.

The volume growth rate observed from 20 to 100 °C was similar to the growth rate observed from 100 to 200 °C, and the rate reached a value of 1.05% at 200 °C. The volume growth rate was then increased slowly from 200 to 300 °C and reached 1.09% at 300 °C. Volume expansion observed within this range of temperatures mainly occurred due to mineral expansion. The volume growth rate plateaued at 300–400 °C, and the volume of the rock specimens did not increase significantly. Above 400 °C, the volume growth rate of the rock specimens began to increase again as the minerals expanded further, and mineral boundaries cracked. The volume growth rate observed at 400–500 °C was similar to that observed at 500–600 °C, and the rate reached a value of 1.46% at 600 °C. Above 600 °C, the volume growth rate increased considerably, because the quartz transformed from the α phase to the β phase at close to 573 °C, and volumes increased rapidly. At this point, transgranular cracks developed rapidly and expanded further, leading to an increase in volume. The volume growth rate observed at 600–800 °C was similar to that observed at 800–1000 °C, and the rate reached a value of 3.61% at 800 °C and a value of 5.63% at 1000 °C.

Density levels were affected by the combined effects of mass and volume changes. Below 200 °C, mass values decreased considerably, while volumes increased significantly, meaning that density reduction processes were also significant. At this point, the density reduction rate was measured to be 1.02%. At 200–600 °C, the mass loss value was small, and volume growth was not obvious; thus, the density reduction rate plateaued, and the density reduction rate reached a value of 1.38%. Above 600 °C, the mass and volume values underwent dramatic changes, and the density reduction rate thus also increased considerably, while the density reduction rate increased to 5.56% at 1000 °C. The density reduction rate observed is consistent with the change observed in volume growth rates, indicating that volume expansion had a greater effect on density than quality losses.

The values of η_m, η_V, and η_ρ are average values for the 12 specimens recorded after each temperature treatment.

3.4 Longitudinal Wave Velocity and Waveform

As shown in Fig. 4, before a temperature of 500 °C was reached, the longitudinal wave velocity decreased linearly with increasing temperatures, and the wave velocity decreased by 46.1% at 500 °C. At 600 °C, the velocity of the longitudinal wave suddenly decreased by 76.9%. The longitudinal wave could no longer be detected at 800 °C and 1000 °C. This finding shows that the rock specimens underwent significant physical and chemical changes at 600 °C that affected the propagation of longitudinal waves. We found 500 °C to be the threshold of longitudinal wave velocity change.

As shown in Fig. 5, the longitudinal wave patterns observed at 100 °C were similar to those originally observed, and the amplitude of longitudinal waves of

Fig. 4 Longitudinal wave velocity changes with changes in temperature

$$y = -4.6766x + 4893.4$$
$$R^2 = 0.9967$$
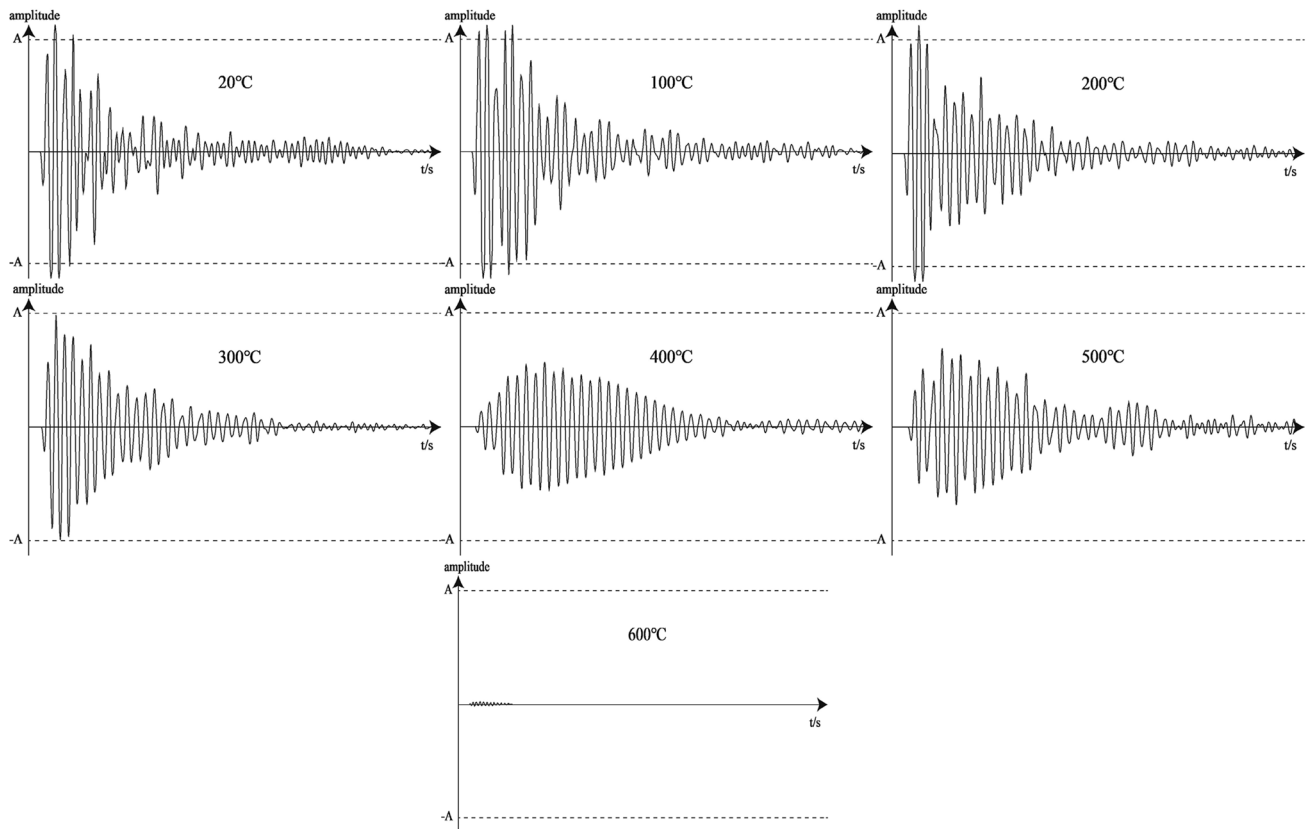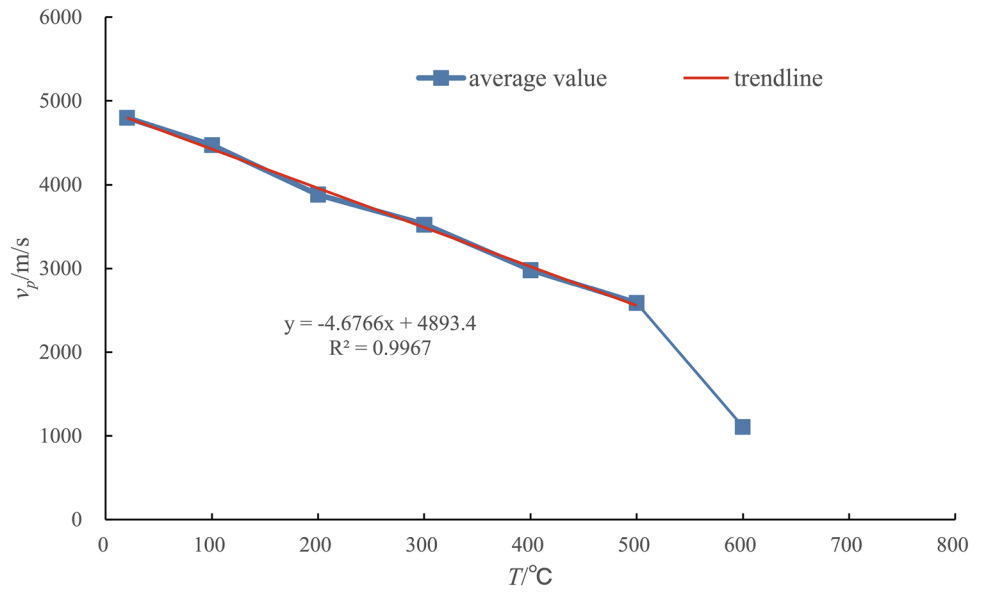
Fig. 5 Longitudinal waveforms of granite observed after 0–600 °C treatment

granite observed above 200 °C decreased with increasing temperatures. The amplitude of the longitudinal wave was close to zero at 600 °C but could still be detected, while the waves were not detectable at 800 °C. Liu and Xu (2015) found that longitudinal waves can still be detected at 800 °C and 1000 °C, which may be attributed to different sources of granite.

The wave velocity and amplitude of the longitudinal wave gradually decreased as temperatures increased, indicating that acoustic wave energy levels were gradually reflected

and absorbed into the rock specimens. This phenomenon occurred for the following reasons. (1) Below 300 °C, temperatures spurred water loss and granite volume growth, which increased the porosity of the granite. Energy levels of the longitudinal wave dissipated during propagation, which led to a decrease in wave velocity and amplitude. (2) At 400–500 °C, more water was lost, and boundary cracks began to appear at mineral boundaries, causing the wave velocity and amplitude to decrease further. (3) At 600 °C, minerals underwent severe physical and chemical changes, and crystals formed transgranular cracks. At this point, the amplitude of the longitudinal wave was very small, and the wave velocity was very low, indicating that cracks absorbed most of the energy in the longitudinal wave. (4) At 800 °C, the effects of high temperatures were more severe, and transgranular cracks developed rapidly and even fused to the mesh. The internal structures of the rock specimens were severely damaged, causing the longitudinal waves to be fully reflected and absorbed and unable to penetrate the rock specimens. Therefore, declines in mass, increases in porosity, the development of transgranular cracks, and the development of boundary cracks spurred a decrease in longitudinal wave velocity. The fusion of transgranular cracks directly caused longitudinal waves to fail to penetrate the rock specimens.

3.5 Stress–Strain Relations

As shown in Fig. 6, as temperatures increase, the stress–strain curve of granite becomes more gradual at 100 °C and the compaction stage extends, while the elastic modulus decreases. At 200–300 °C, the compaction stage shortens, the elastic modulus increases, the elastic deformation stage becomes more pronounced and longer, the peak stress level increases, and the peak strain level decreases. Above 400 °C, the rock specimens soften, the peak stress
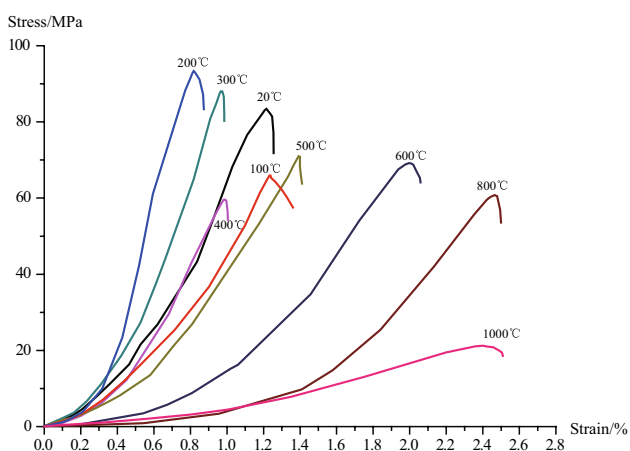
Fig. 6 Uniaxial stress–strain curves for granite after different forms of temperature treatment

of the rock specimens decreases, the elastic deformation stage becomes more gradual, and the peak strain level increases. At 600 °C in particular, the peak strain level clearly increases. At 1000 °C, the rock specimen strength is virtually lost.

Due to a loss of moisture, at 100 °C, voids between the mineral particles expand, and the specimens thus soften slightly. At 200–300 °C, minerals expand, and mineral particles become more tightly intertwined (Huang et al. 2017). Therefore, the rock specimens exhibited hardening characteristics and heightened strength and levels of deformability. Clear boundary cracks appeared on the minerals at 400 °C and 500 °C, causing the stress–strain curve to extend in the compaction stage, presenting obvious softening characteristics. At 600 °C and above, transgranular cracks formed in the granite, and structures within the rock specimens changed, leading to a further decrease in strength and a significant increase in the peak strain level. At 800 °C, macroscopic cracks appeared in the specimens, and intergranular cracks were reticular, decreasing strength and deformability levels, and the specimens presented softened features. At 1000 °C, surface cracks within the rock specimens increased in number and expanded, and the rock specimens rapidly decreased in strength.

3.6 Elastic Modulus, Peak Deviation Stress, and Peak Strain

As shown in Fig. 7, the granite was approximately 15% weaker at 100 °C than it was originally, and its strength was slightly enhanced at 200 °C and 300 °C. At this point, the compressive strength of the specimen was only slightly lower than the original strength value. However, at 400 °C, strength levels suddenly decreased and continued to decrease at 500 °C. The compressive strength measured at 600 °C slightly increased relative to that recorded at 500 °C, but strength levels deteriorated rapidly after a temperature of 600 °C was reached. At 800 °C, the strength levels were approximately 60% those of the undisturbed granite. At 1000 °C, strength levels amounted to only 30% of the original strength value.

The elastic modulus of the granite specimens treated at 100 °C was somewhat lower than that of the undisturbed granite (5.3% lower). The elastic modulus increased at 200 °C and was 23% higher than the original value. At 300 °C, the elastic modulus of granite decreased to the original levels. Once a temperature of 300 °C was reached, the deformability of the granite declined rapidly. At 400 °C, the elastic modulus of granite decreased by 18.3%. At 500 °C and above, the elastic modulus of the granite decreased linearly. At 500 °C, the elastic modulus decreased by 30% relative to the original value and decreased by approximately

Fig. 7 Relationships between uniaxial compressive strength, elastic modulus, and peak strain values and temperatures
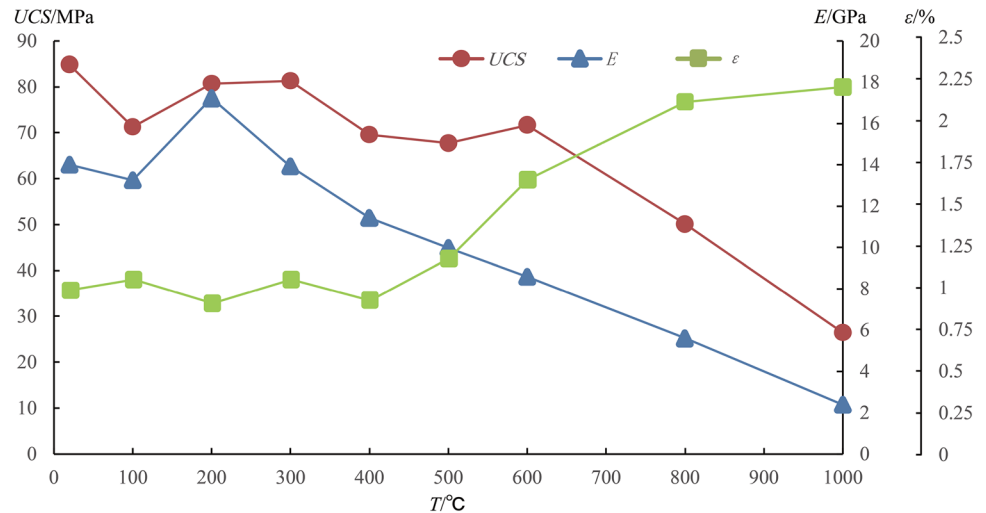
85% at 1000 °C. At this point, the deformation capacities of the granite had deteriorated considerably.

As shown in Fig. 7, the peak strain values increased and fell before 400 °C, primarily due to a loss of moisture and the expansion of minerals. At temperatures above 500 °C, the peak strain value increased rapidly with increasing temperatures, because high temperatures spurred the formation of more cracks within the granite, softening the rock specimen. At 500 °C, the peak strain value started to increase significantly by approximately 20.4%. At 600 °C, the peak strain value increased significantly by approximately 68.4%. The peak strain growth rate observed at 800 °C and 1000 °C was slower than that at lower temperature. The peak strain level observed at 800 °C represented an increase of approximately 115% to twice the value of the original peak strain, and the peak strain observed at 1000 °C represented an increase of approximately 124%.

Most scholars have concluded that as temperatures increase, both the strength and elastic modulus decrease. However, some scholars have shown that the strength and deformability of granite increase at 200 °C (Shao et al. 2015; Liu and Xu 2015; Chen et al. 2017). Yang et al. (2017a, b) found that the strength and elastic modulus of granite at 300 °C are higher than those of undisturbed granite. Huang et al. (2017) observed that primary cracks in granite are closed at 150 °C, strengthening the granite structure. Once a temperature of 300 °C is reached, the mineral boundary cracks and the structures are damaged. These findings echo our results; thus, the influence of granite source on the mechanical properties of granite cannot be ignored.

Through the change laws of compressive strength, elastic modulus, and peak strain values, we may speculate that at 100 °C, due to a loss of interlayer water, the porosity of the granite specimens increased, such that strength and deformability values were reduced, while the peak strain value slightly increased. At 200–300 °C, mineral expansion accounted for pores due to moisture loss, and mineral particles became more compact. Thus, as compressive strength levels increased, deformability levels also increased, causing the peak strain to decline. At temperatures between 400 and 600 °C, the boundary between minerals cracked, rock strength declined rapidly, deformability levels declined, and the peak strain value increased rapidly. After a temperature of 600 °C was reached, transgranular cracks developed rapidly in the minerals. At 800 °C in particular, transgranular cracks were meshed, resulting in a rapid loss of rock strength, weakened deformation ability, and a rapid increase in peak strain values.

As shown in Fig. 8, at 400 °C, under confining pressure, the elastic modulus did not change significantly with temperature and decreased above 600 °C. Two different patterns compared with those of the uniaxial condition were observed. (1) In the uniaxial state, the elastic modulus of granite increased at 200 °C and later decreased. However, when the confining pressure level was 5 MPa, the elastic modulus of granite increased from 200 °C, decreased slightly at 400 °C, and reached a maximum value at 600 °C. At this point, the growth rate was approximately 94%, and it subsequently decreased after a temperature of 600 °C was reached. (2) When the confining pressure reached 10 MPa or 15 MPa, the elastic modulus slowly declined below 400 °C, while it deteriorated rapidly at temperatures of 400 °C and above.

When the temperature was below 200 °C and the confining pressure was 5 MPa, the change laws of elastic modulus were similar to that of the uniaxial condition. The main reason for this change was that the water loss could increase the porosity and weaken connections among mineral grains in the rock. When the confining pressure was 10 MPa or 15 MPa, elastic modulus changed little due to the closure of voids induced by the water loss. When the temperature rose from 300 to 500 °C, elastic modulus also changed little

Fig. 8 Relationships between elastic modulus and temperature values observed under different confining pressure levels
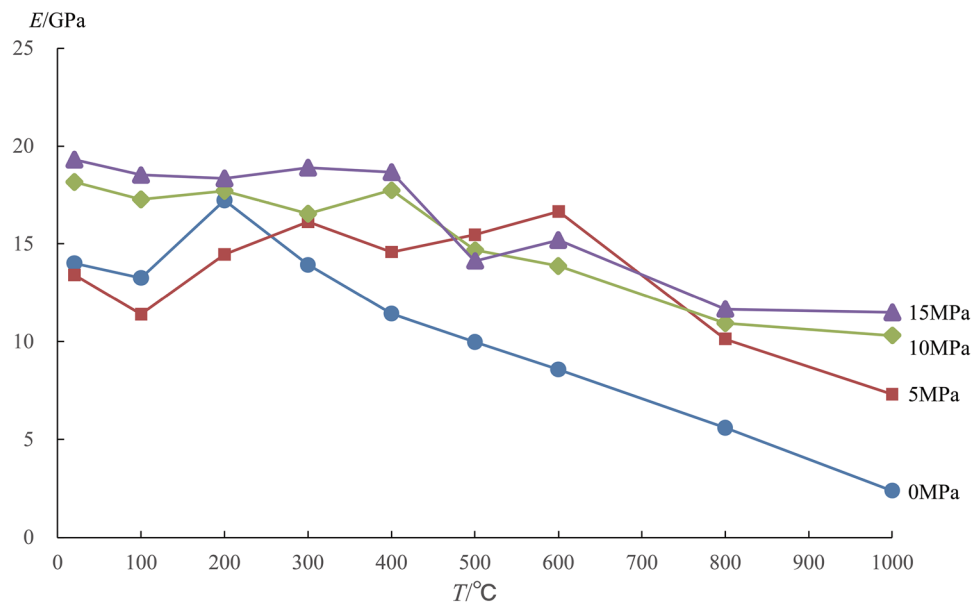

owing to the closure of boundary cracks under the confining pressure. However, when the temperature reached 600 °C, elastic modulus was affected more obviously by the transgranular cracks rather than the confining pressure, and the elastic modulus decreased under different confining pressure.

Under triaxial conditions (Fig. 9), the peak deviation stress of granite observed at temperatures below 400 °C did not change considerably and decreased slightly before a temperature of 300 °C was reached and increased after a temperature of 300 °C was reached. In contrast to the changes observed under uniaxial conditions, the peak deviation stress

observed under triaxial conditions was not greatly reduced after a temperature of 600 °C was reached, echoing results obtained for the undisturbed granite. When the confining pressure reached 5 MPa or 15 MPa, the elastic modulus suddenly increased at 600 °C (Fig. 8). Moreover, the peak deviation stress also increased at 600 °C under various confining conditions (Fig. 9). Thus, we speculated that despite the minerals cracking at 600 °C, the frictional characteristics of the mineral particles were enhanced. In particular, the cracks were closed under confining pressures, which increased the strength and elastic modulus levels. When a temperature of

Fig. 9 Relationships between peak deviation stress and temperature values observed under different confining pressure levels
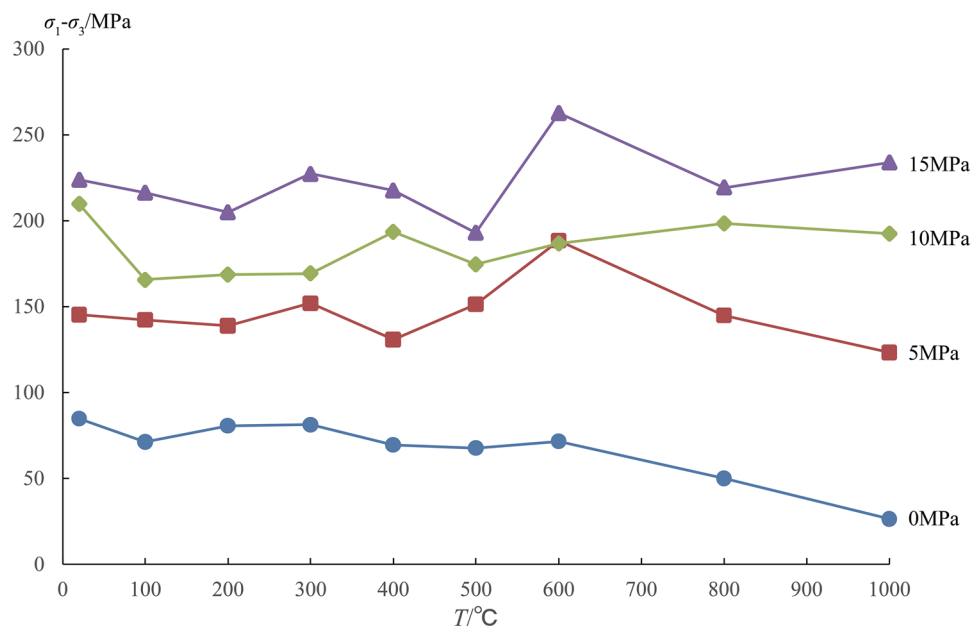
800 °C was reached, the cracks were connected and meshed, resulting in a little decrease of the compressive strength.

As shown in Fig. 10, peak strain levels increased and decreased below 400 °C, but these changes were not significant. The peak strain increased rapidly after 500 °C. Under the dual effects of temperature and confining pressure in particular, the rock specimens softened, while the peak strain markedly increased. For example, when the confining pressure was 5 MPa, the peak strain of the rock specimens observed after treatment at 1000 °C was approximately 3.2 times that of the original.

Under the influence of confining pressure, changes in the mechanical properties of the granite were not clearly affected by temperature as much as they were under uniaxial conditions. Even in terms of compressive strength, few changes from the original values were observed with only a slight decrease in the elastic modulus. However, the increase in peak strain was much more obvious than that observed under uniaxial conditions, indicating that the strength of the granite was greatly affected by the confining pressure, while the influence of temperatures on deformation capacities was more pronounced.
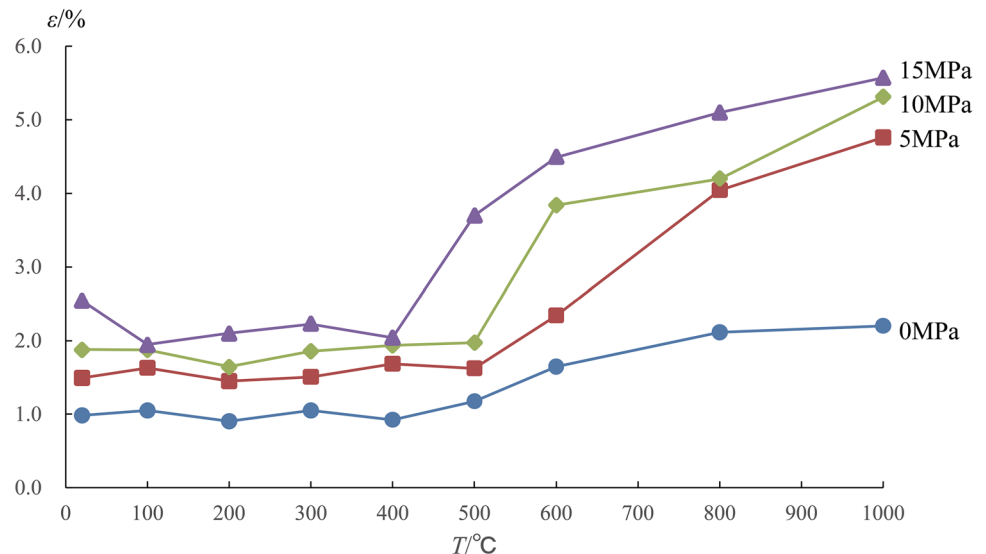
3.7 Cohesion and Friction Angle

At 100 °C, relative to that of the undisturbed granite, cohesion decreased by 12.6% and recovered at 200 °C, but decreased at 300 °C. At this point, cohesion had declined by 2.3% compared to the original values. At 400 °C, cohesion rapidly decreased by approximately 19.8%. At 500 °C, cohesion quickly recovered. At this point, cohesion was not markedly different from that of the undisturbed granite. Thereafter, as temperatures increased, cohesion gradually decreased by 9.5% at 600 °C, by 31.3% at 800 °C, and by 63.6% at 1000 °C relative to the original.

Compared to that of the undisturbed granite, the friction angle observed at 100 °C slightly decreased, and it continued to decrease at 200 °C, but it increased slightly at 300 °C and 400 °C. This angle later decreased again at 500 °C. At temperatures of 500 °C and above, as temperatures increased, the friction angle gradually increased. At temperatures below 500 °C, the friction angle did not change significantly and remained relatively stable overall. The friction angle increased by approximately 4.3% at 600 °C and by approximately 8.9% at 1000 °C.

Cohesion reflects the degree of cementation within a rock specimen, and the internal friction angle reflects the frictional properties of rock. Based on the above-mentioned results, we may speculate that cohesion decreased at 100 °C due to a loss of interlayer water, although the observed changes were minor. At 200 °C, the volume of the mineral expanded, and the volume of rock specimen increased (Fig. 3), which strengthened the structure and increased cohesion. At 300 °C, microcracks appeared, leading to a slight increase in the internal friction angle and a decrease in cohesion. Below 300 °C, the loss of interlayer and zeolite water did not cause major changes in cohesion and friction angle values. At 400 °C, due to the generation of intercrystalline cracks, cohesion declined rapidly, while frictional properties were improved, resulting in an increase in the friction angle. At 500 °C, the minerals obviously expanded, causing the volume of the specimens to increase further (Fig. 3), which strengthened the structure of the rock specimens, and the cohesion increased again. After treatment at 600 °C, the minerals broke, and the fracture surfaces pressed against each other, leading to an increase in the friction properties and friction angle. At 800 °C and 1000 °C, the rupture surface penetrated, making the mutual locking effect more obvious (Fig. 11).

Fig. 10 Relationships between peak strain and temperature values observed under different confining pressure conditions

3.8 Damage Parameters

The damage parameters $D(v_p)$, $D(\text{UCS})$, $D(E)$, $D(\varepsilon)$, $D(\varphi)$, and $D(c)$ are expressed in terms of the longitudinal wave velocity, uniaxial compressive strength, elastic modulus, peak strain, internal friction angle, and cohesion as follows:

$$D(v_p) = \frac{(v_{p0} - v_{pT})}{v_{p0}} \times 100\%,$$

$$D(\text{UCS}) = \frac{(\sigma_0 - \sigma_T)}{\sigma_0} \times 100\%,$$

$$D(E) = \frac{(E_0 - E_T)}{E_0} \times 100\%,$$

$$D(\varepsilon) = \frac{(\varepsilon_T - \varepsilon_0)}{\varepsilon_0} \times 100\%,$$

$$D(\varphi) = \frac{(\varphi_T - \varphi_0)}{\varphi_0} \times 100\%,$$

$$D(c) = \frac{(c_0 - c_T)}{c_0} \times 100\%.$$

Parameters with subscript 0 in the formula denote data obtained from the original granite specimen. Parameters with subscript T in the formula denote data obtained from granite treated at each temperature.

As shown in Fig. 12, physical and mechanical parameters were enhanced with increasing temperatures, and the primary changes were observed. (1) The damage factor defined by the longitudinal wave velocity was the most sensitive, especially because the longitudinal wave velocity could not be measured after 600 °C; hence, damage values could not be defined. (2) Changes observed in the various damage factors show that the granite damage observed can be categorized into four stages. At temperatures below 200 °C, the damage factors first increased and later decreased due to a loss of water and the expansion of minerals. At 200–400 °C, the damage factors first decreased and then increased, indicating that mechanical properties were first strengthened, but

Fig. 11 Variation in friction angle and cohesion with temperature
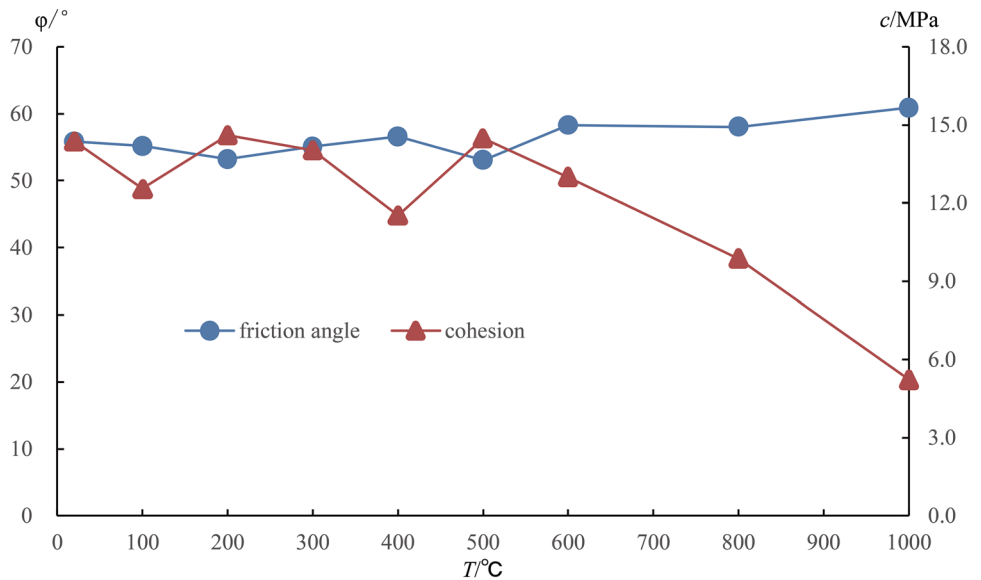
Fig. 12 Relationships between damage parameters and temperature
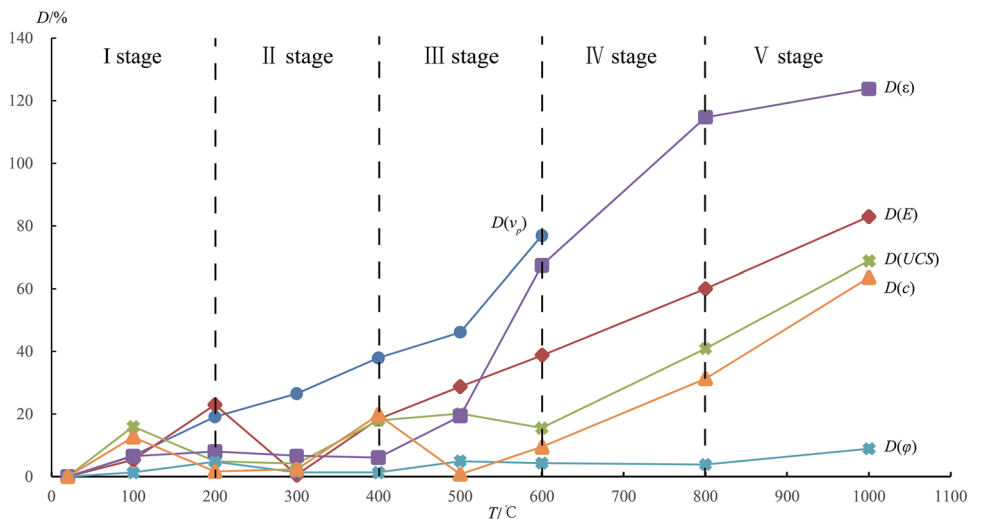
due to the generation of intercrystalline cracks, mechanical properties then immediately deteriorated. At 400–600 °C, the damage factors increased, indicating that the granite continued to be damaged at these temperatures. At temperatures exceeding 600 °C, various damage factors increased rapidly, indicating that damage developed rapidly at these temperatures. (3) The damage factor defined by the internal friction angle did not increase considerably below 1000 °C, indicating that temperatures did not have a considerable influence on the friction properties of the rock specimens.

Zhang et al. (2016) studied changes observed in the physical and mechanical properties of granite below 500 °C and defined changes observed based on three temperature stages: room temperature to 100 °C, 100–300 °C, and 300–500 °C. Gautam et al. (2018) concluded that 300 °C is the damage threshold temperature for the thermophysical properties of granite. Xu and Zhang (2018) studied acoustic emission and damage characteristics of granite observed at below 1000 °C and defined temperature effects observed based on four stages: room temperature to 400 °C, 400–600 °C, 600–800 °C, and 800–1000 °C. Hu et al. (2018) defined temperature effects observed below 1000 °C into four stages: room temperature to 200 °C, 200–400 °C, 400–600 °C, and 600–1000 °C. Owing to different sources of granite, the experimental results reported by different researchers vary, although the temperatures used to define the different stages are largely the same. According to the above-mentioned experimental phenomena, based on the results of previous studies, we divided the change processes of granite into five stages according to temperature. (1) At room temperature to 200 °C, granite oxidation was not obvious, and mass loss was caused by a loss of interlayer water. At this point, the mechanical properties declined slightly. (2) At 200–400 °C, mass loss was caused by a loss of zeolite water, and minerals expanded into original pores, resulting in the strengthening of the granite structure and the intensification of mechanical properties. (3) At 400–600 °C, a loss of mass was caused by a loss of crystal water, and cracks appeared at mineral boundaries, quickly decreasing the longitudinal wave velocity and clearly weakening mechanical properties. (4) At 600–800 °C, mass loss was mainly caused by a loss of crystal and structural water. Minerals formed transgranular cracks, the crystal phase of quartz changed, the volume of the rock specimen increased, and the longitudinal wave did not penetrate the granite at this stage. At this stage, the mechanical properties of the granite were softened. (5) At 800–1000 °C, the rock specimens underwent significant chemical changes. Transgranular cracks were connected into the mesh, and the structure was severely damaged. Macroscopic cracks appeared on the surface of the rock specimens. Deformation essentially involved plastic deformation, and mechanical properties deteriorated considerably.

From the above analysis, it can be concluded that the physical and mechanical properties of granite undergo a major transformation at 400 °C, 600 °C, and 800 °C, indicating that these three temperatures are characteristic temperatures that spur changes in the physical and mechanical properties of granite. Above 600 °C, the mechanical properties of granite deteriorate; thus, 600 °C is the change threshold for mechanical properties.
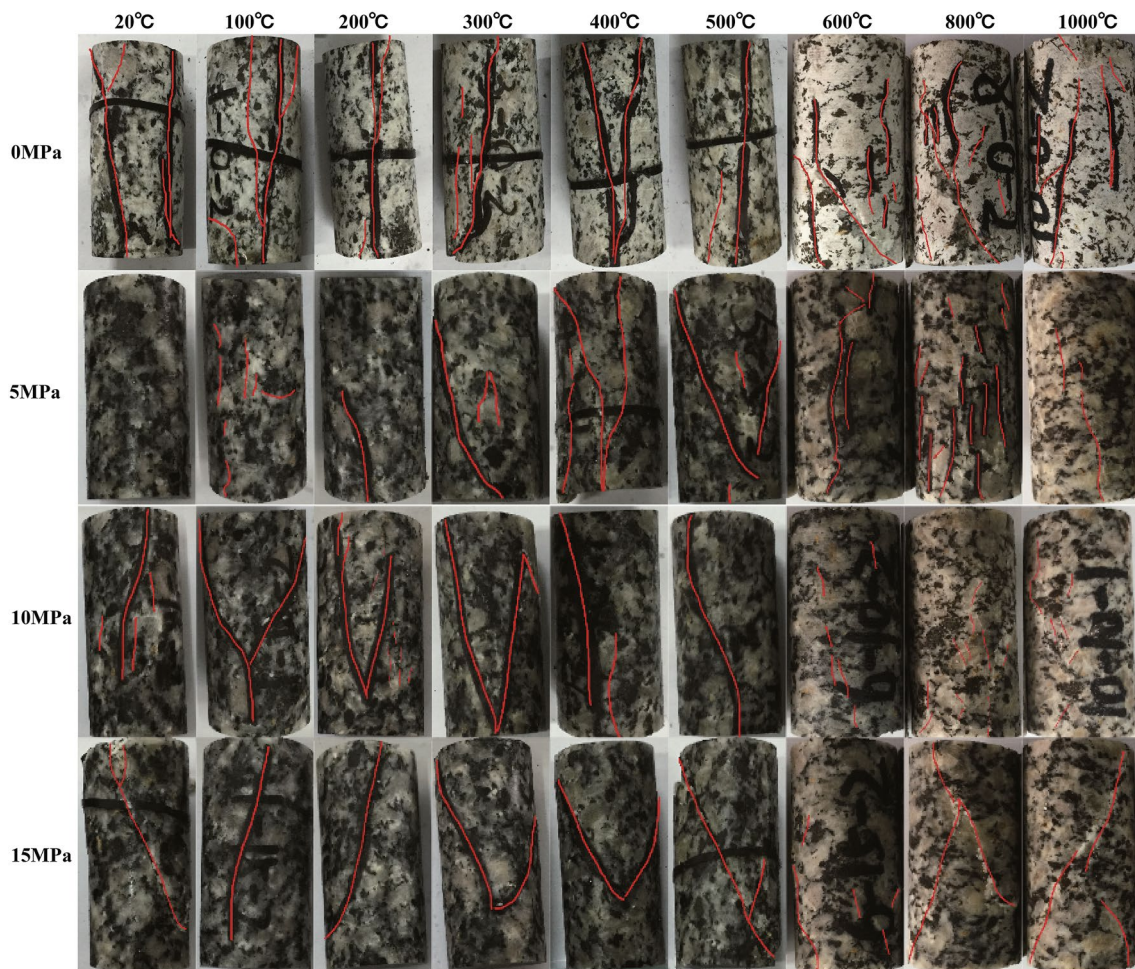
3.9 Failure Pattern

Figure 13 shows that in the uniaxial state, the rock specimens underwent shear failure at temperatures below 500 °C, while fractures formed within the rock specimens. At 600 °C and above, no obvious fractures were observed in the rock specimens, but more cracks appeared on the surfaces of the rock specimens, indicating that the rocks underwent plastic failure. This phenomenon was observed, because boundary and transgranular cracks formed within the rocks at 600 °C. Therefore, plastic failure occurred under external loads. We identified 600 °C as the failure transformation temperature for granite.

Under triaxial conditions, the specimens treated at temperatures below 500 °C exhibited shear failure. For the specimens treated at 600–1000 °C, a transition to plastic failure occurred at 5 MPa and 10 MPa. When the confining pressure was set to 15 MPa, the rock specimens underwent plastic and shear failure. Due to a loss of moisture within the rock specimen after high-temperature treatment, cohesion levels declined, and cracks formed within and on the surface of the rock specimens. In turn, plastic failure easily occurred. However, under high confining pressure levels, pores, and cracks within the rock specimens closed, while a number of the rock specimens underwent shear failure.

3.10 Comparison with Other Research

Many experimental methods such as acoustic emission and compression test have been used to study the physical and mechanical properties of granite after high-temperature treatment. However, different sources of granite and experimental methods can contribute to different experimental results. Due to the data limitation of the physical properties, such as mass, volume, and density of granite after high-temperature treatment, and the mechanical properties under triaxial conditions in the literatures, here, we just show the summary of longitudinal wave velocity, uniaxial compressive strength, elastic modulus, and uniaxial peak strain in Fig. 14. And we also sum up the mineral composition of granite in the previous literatures and this study (Table 2).

As shown in Fig. 14a, the longitudinal wave velocity decreases with the temperature increasing. Liu and Xu (2014, 2015) find that the longitudinal wave velocity

Fig. 13 Failure pattern of granite under different confining pressure levels after treatments at different temperatures

increases at 100 °C. However, with the temperature increasing to 800 °C and 1000 °C, we could not detect the longitudinal wave that could be detected by Liu and Xu (2014, 2015) and Yang et al. (2017a, b), which may be due to the different mineral composition. As listed in Table 2, the quartz content in granite researched by Liu and Xu (2014, 2015) and Yang et al. (2017a, b) is less than 20% which is much lower than 38% quartz in this study. More quartz contents lead to more cracks in granite when the temperature is above 600 °C, which causes the disappearance of longitudinal wave at 800 °C and 1000 °C.

Figure 14b–d shows all the test results obtained by the researchers. With the temperature increasing, the compressive strength and the elastic modulus decrease, while the peak strain increases. However, Chen et al. (2017) and Yang et al. (2017a, b) find that the elastic modulus fell to a low level (<8% that of undisturbed granite) (Fig. 14c), while the peak strain increases rapidly in Yang et al. (2017a, b) (Fig. 14d) at 600 °C. The peculiarity of the granite in Yang et al. (2017a, b) and Chen et al. (2017) is the lower composition of quartz

than in the other research. Therefore, we can infer that quartz contributes more to the elastic modulus of granite than feldspar, which means the lower quartz content may cause the lower elastic modulus and the larger peak strain. Furthermore, no obvious difference has been found in the comparison of the compressive strength (Fig. 14b) when the quartz content changes in different research. That means feldspar, another main mineral, has more influences on the strength for all studies which have similar feldspar content. However, more detail tests need to be conducted in the next research.

4 Conclusions

In this study, the changes in the physical and mechanical properties of granite observed at room temperature to 1000 °C were examined through a series of tests, and the corresponding change rules and relations were analyzed. Our main conclusions are as follows:
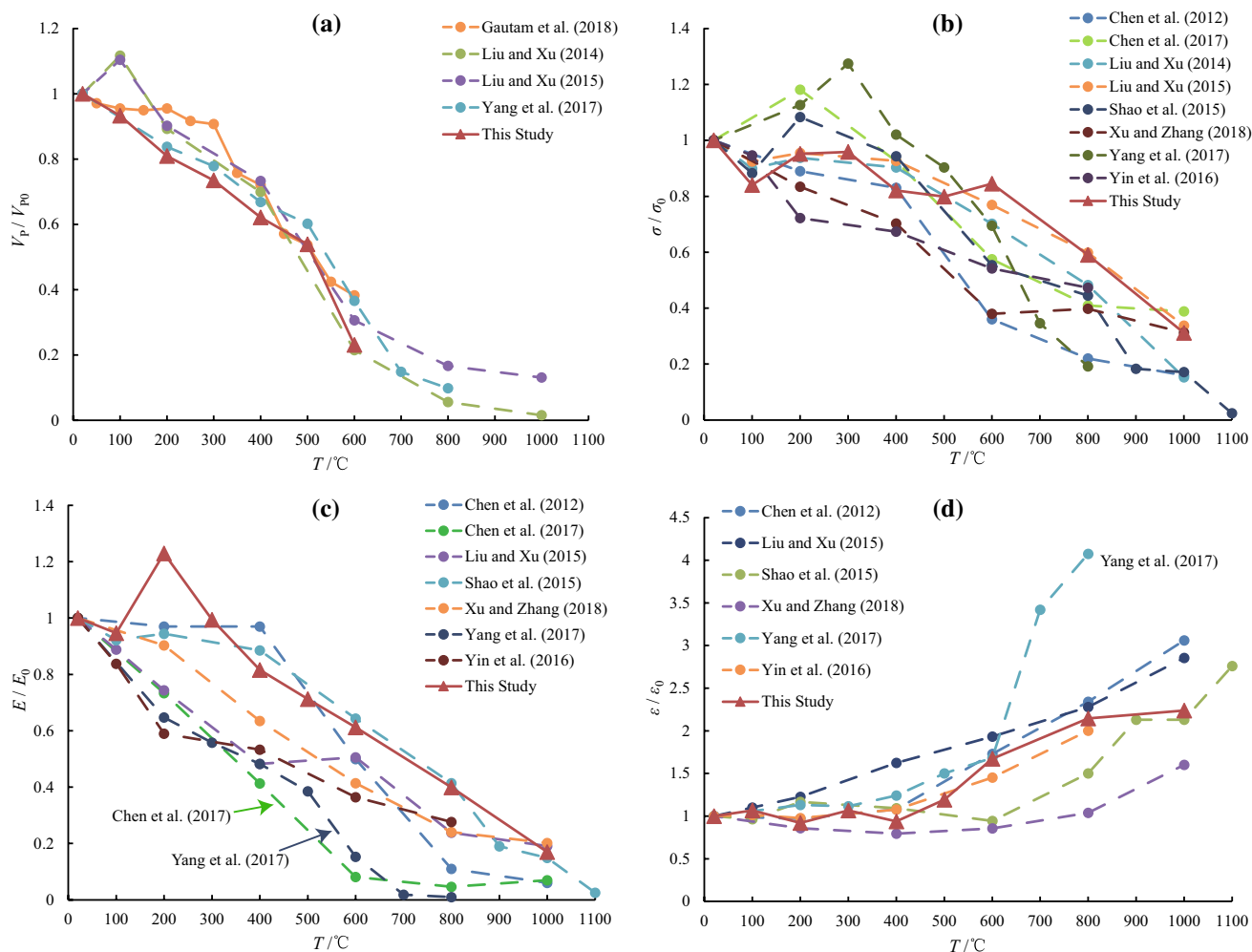
Fig. 14 Relationships between V_P/V_{P0}, σ/σ_0, E/E_0, and $\varepsilon/\varepsilon_0$ and temperature

Table 2 Mineral composition in the previous literatures and this study

Reference	Quartz, %	Feldspar, %	Other minerals, %
Chen et al. (2012)	28.3	61.6	10.1
Chen et al. (2017)	15–20	45–50	30–40
Liu and Xu (2014, 2015)	17	45	38
Yang et al. (2017a, b)	11.2	59.85	28.95
Yin et al. (2016)	46.54	37.95	15.51
This study	38	58	4

1. High temperatures affect the physical properties of granite by spurring thermal cracking on the appearance of specimens (at 800 °C and 1000 °C), leading to a decline in density, which is mainly caused by the loss of water and an increase in volume; by decreasing density rapidly above 600 °C; by causing the recrystallization and

alteration of minerals (above 600 °C); and by causing mineral cracking (above 400 °C).

2. At temperatures below 500 °C, longitudinal wave velocities decrease (46.1%), amplitudes decrease, and longitudinal wave energy is gradually absorbed. With 600 °C as the threshold temperature, the wave velocity and amplitude of the longitudinal wave rapidly decrease (76.9%). When the temperature reaches 800 °C, the longitudinal wave cannot be detected.

3. Below 400 °C, E, UCS, and ε change little. However, E declines rapidly and ε increases rapidly after 400 °C, while *UCS* remains unchanged until 600 °C. Above 600 °C, UCS also declines rapidly. The friction angle changes little at temperatures below 1000 °C. Below 500 °C, cohesion only declines at 100 °C and 400 °C, while at other temperatures, cohesion remains at a similar level. Above 500 °C, cohesion declines with increasing temperature. All damage parameters change little below 400 °C and increase rapidly after 400 °C, except

for the factor defined by friction angle. When the temperature is 400 °C, the values of $D(v_p)$, D(UCS), $D(E)$, $D(\varepsilon)$, $D(\varphi)$, and $D(c)$ are 37.87%, 18.36%, 17.94%, 6.08%, 1.31%, and 19.81%, respectively. When the temperature reaches 1000 °C, $D(v_p)$ no longer exists, while the values of the other parameters are 82.97%, 68.83%, 123.76%, 8.94%, and 63.61%, respectively.

4. With an increase in temperature, the stress–strain curve first hardens and later softens. The mechanical properties change little at temperatures below 400 °C. Once temperatures exceed 500 °C, the compressive strength and elastic modulus decrease rapidly. At 1000 °C, the granite specimens largely lose their bearing capacity and deformability. We found 600 °C to be the change threshold temperature of mechanical properties and of the failure pattern.

5. At 400 °C, the boundary cracks among the crystals and the mechanical properties are slightly weakened. At 600 °C, the crystal phase of quartz changes and transgranular cracks form. In turn, the mechanical properties of granite deteriorate rapidly. At 800 °C, macroscopic cracks appear on the surfaces of rock specimens, and transgranular cracks broaden and become interconnect, resulting in a serious loss of compressive strength and deformability. Therefore, temperatures of 400 °C, 600 °C, and 800 °C are identified as the characteristic temperatures that shape the physical and mechanical properties of granite.

References

Basu A, Mishra DA, Roychowdhury K (2013) Rock failure modes under uniaxial compression, Brazilian, and point load tests. Bull Eng Geol Environ 72(3–4):457–475

Brotons V, Tomás R, Ivorra S, Alarcón JC (2013) Temperature influence on the physical and mechanical properties of a porous rock: San Julian's calcarenite. Eng Geol 167:117–127

Chen YL, Ni J, Shao W, Azzam R (2012) Experimental study on the influence of temperature on the mechanical properties of granite under uni-axial compression and fatigue loading. Int J Rock Mech Min 56:62–66

Chen YL, Wang SR, Ni J, Azzam R, Fernandez-Steeger TM (2017) An experimental study of the mechanical properties of granite after high temperature exposure based on mineral characteristics. Eng Geol 220:234–242

Chmel A (2013) A comparative acoustic emission study of compression and impact fracture in granite. Int J Rock Mech Min 64:56–59

Costamagna R, Renner J, Bruhns OT (2007) Relationship between fracture and friction for brittle rocks. Mech Mater 39(4):291–301

Dwivedi RD, Goel RK, Prasad VVR, Sinha A (2008) Thermo-mechanical properties of Indian and other granites. Int J Rock Mech Min 45(3):303–315

Ersoy H, Kolaylı H, Karahan M, Karahan HH, Sünnetci MO (2017) Effect of thermal damage on mineralogical and strength properties of basic volcanic rocks exposed to high temperatures. Bull Eng Geol Environ 78(3):1515–1525

Gautam PK, Verma AK, Sharma P, Singh TN (2018) Evolution of thermal damage threshold of Jalore granite. Rock Mech Rock Eng 51(9):2949–2956

Goodman RE (1989) Introduction to rock mechanics, vol 2. Wiley, New York

Hardy HR (1972) Application of acoustic emission techniques to rock mechanics research. In acoustic emission. ASTM International, West Conshohocken

Hawkes I, Mellor M (1970) Uniaxial testing in rock mechanics laboratories. Eng Geol 4(3):179–285

Homand-Etienne F, Houpert R (1989) Thermally induced microcracking in granites: characterization and analysis. Int J Rock Mech Min 26(2):125–134

Hoxha D, Homand F (2000) Microstructural approach in damage modeling. Mech Mater 32(6):377–387

Hu J, Sun Q, Pan X (2018) Variation of mechanical properties of granite after high-temperature treatment. Arab J Geosci 11(2):43

Huang YH, Yang SQ, Tian WL, Zhao J, Ma D, Zhang CS (2017) Physical and mechanical behavior of granite containing pre-existing holes after high temperature treatment. Arch Civ Mech Eng 17(4):912–925

ISRM (2007) The complete ISRM suggested methods for rock characterization, testing and monitoring: 1974–2006. International Society for Rock Mechanics, Commission on Testing Methods

Kawakata H, Cho A, Kiyama T, Yanagidani T, Kusunose K, Shimada M (1999) Three-dimensional observations of faulting process in Westerly granite under uniaxial and triaxial conditions by X-ray CT scan. Tectonophysics 313(3):293–305

Kumari WGP, Ranjith PG, Perera MSA, Shao S, Chen BK, Lashin A, Rathnaweera TD (2017) Mechanical behaviour of Australian Strathbogie granite under in situ stress and temperature conditions: an application to geothermal energy extraction. Geothermics 65:44–59

Liu S, Xu J (2013) Study on dynamic characteristics of marble under impact loading and high temperature. Int J Rock Mech Min 62:51–58

Liu S, Xu J (2014) Mechanical properties of Qinling biotite granite after high temperature treatment. Int J Rock Mech Min 71:188–193

Liu S, Xu J (2015) An experimental study on the physico-mechanical properties of two post-high-temperature rocks. Eng Geol 185:63–70

Liu X, Yuan S, Sieffert Y, Fityus S, Buzzi O (2016) Changes in mineralogy, microstructure, compressive strength and intrinsic permeability of two sedimentary rocks subjected to high-temperature heating. Rock Mech Rock Eng 49(8):2985–2998

Mao R, Mao X, Zhang L, Liu R (2015) Effect of loading rates on the characteristics of thermal damage for mudstone under different temperatures. Int J Min Sci Technol 25(5):797–801

Mitchell EK, Fialko Y, Brown KM (2016) Velocity-weakening behavior of Westerly granite at temperature up to 600 °C. J Geophys Res: Solid Earth 121(9):6932–6946

Rudajev V, Vilhelm J, Lokajíček T (2000) Laboratory studies of acoustic emission prior to uniaxial compressive rock failure. Int J Rock Mech Min 37(4):699–704

Scherbakov IP, Chmel AE (2014) Impact fracture of granite at temperatures from 20 to 500 °C. Russ Geol Geophys 55(10):1223–1228

Shao S, Wasantha PLP, Ranjith PG, Chen BK (2014) Effect of cooling rate on the mechanical behavior of heated Strathbogie granite with different grain sizes. Int J Rock Mech Min 70:381–387

Shao S, Ranjith PG, Wasantha PLP, Chen BK (2015) Experimental and numerical studies on the mechanical behaviour of Australian Strathbogie granite at high temperatures: an application to geothermal energy. Geothermics 54:96–108

Sirdesai NN, Singh A, Sharma LK, Singh R, Singh TN (2018) Determination of thermal damage in rock specimen using intelligent techniques. Eng Geol 239:179–194

Su G, Chen Z, Ju JW, Jiang J (2017) Influence of temperature on the strainburst characteristics of granite under true triaxial loading conditions. Eng Geol 222:38–52

Takarli M, Prince W, Siddique R (2008) Damage in granite under heating/cooling cycles and water freeze–thaw condition. Int J Rock Mech Min 45(7):1164–1175

Tian H, Kempka T, Xu NX, Ziegler M (2012) Physical properties of sandstones after high temperature treatment. Rock Mech Rock Eng 45(6):1113–1117

Tian H, Ziegler M, Kempka T (2014) Physical and mechanical behavior of claystone exposed to temperatures up to 1000 °C. Int J Rock Mech Min 70:144–153

Tian H, Kempka T, Yu S, Ziegler M (2016) Mechanical properties of sandstones exposed to high temperature. Rock Mech Rock Eng 49(1):321–327

Tian H, Mei G, Jiang GS, Qin Y (2017) High-temperature influence on mechanical properties of diorite. Rock Mech Rock Eng 50(6):1661–1666

Vázquez P, Shushakova V, Gómez-Heras M (2015) Influence of mineralogy on granite decay induced by temperature increase: experimental observations and stress simulation. Eng Geol 189:58–67

Xu XL, Zhang ZZ (2018) Acoustic emission and damage characteristics of granite subjected to high temperature. Adv Mater Sci Eng 2018:8149870

Xu XL, Gao F, Zhang ZZ, Zhang CH (2014) Energy and structural effects of granite after high temperature. Chin J Geotech Eng 36(5):961–968 **(in Chinese)**

Yang SQ, Ranjith PG, Jing HW, Tian WL, Ju Y (2017a) An experimental investigation on thermal damage and failure mechanical behavior of granite after exposure to different high temperature treatments. Geothermics 65:180–197

Yang SQ, Xu P, Li YB, Huang YH (2017b) Experimental investigation on triaxial mechanical and permeability behavior of sandstone after exposure to different high temperature treatments. Geothermics 69:93–109

Yin TB, Shu RH, Li XB, Pin WANG, Liu XL (2016) Comparison of mechanical properties in high temperature and thermal treatment granite. Trans Nonferrous Met Soc China 26(7):1926–1937

Zhang W, Sun Q, Hao S, Geng J, Lv C (2016) Experimental study on the variation of physical and mechanical properties of rock after high temperature treatment. Appl Therm Eng 98:1297–1304

Zhao Y, Wan Z, Feng Z, Yang D, Zhang Y, Qu F (2012) Triaxial compression system for rock testing under high temperature and high pressure. Int J Rock Mech Min 52:132–138

Zhao XG, Cai M, Wang J, Ma LK (2013) Damage stress and acoustic emission characteristics of the Beishan granite. Int J Rock Mech Min 64:258–269